Journal of Innovative Optical Health Sciences
Vol. 5, No. 2 (2012) 1250009 (8 pages)
© World Scientific Publishing Company
DOI: 10.1142/S1793545812500095

World Scientific
www.worldscientific.com

J. Innov. Opt. Health Sci. 2012.05. Downloaded from www.worldscientific.com
by HUAZHONG UNIVERSITY OF SCIENCE AND TECHNOLOGY on 10/24/18. Re-use and distribution is strictly not permitted, except for Open Access articles.

HIGH RESOLUTION, REAL-TIME LINE-FIELD FOURIER-DOMAIN INTERFEROMETRY

QING XIAO and LING FU*
Britton Chance Center for Biomedical Photonics
Wuhan National Laboratory for Optoelectronics-Huazhong
University of Science and Technology
1037 Luoyu Rd., Wuhan 430074, P. R. China

Key Laboratory of Biomedical Photonics of Ministry of Education
Huazhong University of Science and Technology
1037 Luoyu Rd., Wuhan 430074, P. R. China
**lfu@mail.hust.edu.cn*

Received 19 March 2012
Accepted 19 March 2012
Published 3 May 2012

To increase the application potential in manufacturing process, such as monitoring the processing performance, the profile measurement should be provided in real-time display and with high resolution simultaneously. We propose a line-field Fourier-domain interferometric method (LFI), which combines the line-field microscope with spectral interferometer, for the surface cross-sectional profile measurement with no scan needed. The white light and objectives are employed to offer high axial and lateral resolution, respectively. In our system setup, the measurement could be implemented in real-time display of 10 frame/s, and the resolutions of the LFI system in X, Y, and Z directions are $\sim 8\,\mu$m, $\sim 3.2\,\mu$m, and $\sim 1.4\,\mu$m, respectively. As a demonstration, the cross-sectional profiles of a microfluidic chip are tested. The graphics processing unit is also used to accelerate the reconstruction algorithm to achieve the real-time display of the cross-sectional profiles.

Keywords: Line-field; Fourier-domain; interferometry; cross-sectional profile; real-time.

1. Introduction

The surface profile measurement plays an important role in the quality control and performance testing of the manufacturing process.[1–4] For the surface topography testing, the conventional measurement methods, such as scanning electron microscopy (SEM) and atomic force microscopy (AFM) are frequently adopted. SEM could obtain the accurate morphological observation. However, it cannot offer the cross-sectional profile and the depth measurements, and nonconductive specimens need to be coated with a thin film of conducting material. AFM is a suggested tool for the microelectromechanical systems (MEMS) measurement. During the analysis, it is found that AFM is not suitable for the large specimens such as millimeter size and it is time consuming.

Comparatively, optical interferometry has the advantages of noncontact, nondestructive, nonprocessing, and it is potential for the application of monitoring the processing performance. Therefore,

J. Innov. Opt. Health Sci. 2012.05. Downloaded from www.worldscientific.com
by HUAZHONG UNIVERSITY OF SCIENCE AND TECHNOLOGY on 10/24/18. Re-use and distribution is strictly not permitted, except for Open Access articles.

the optical interferometry is a kind of widely developed technique for the measurement of distance, thickness, and material surface profile. White-light interferometry (WLI) is one of the most commonly used methods for the measurement of surface topography[5−9] Based on the Michelson interferometer and using wideband light source, the WLI setup could be used for the 3D structure measurement with no phase ambiguity. However, mechanical scan is required for WLI, and the sampling interval must be lower than the Nyquist interval of the carrier fringe. In practice, the sampling interval of the mechanical scan is usually set to be several tens of nanometers, which means a lot of time will be spent. Therefore, it is difficult for WLI to obtain the surface profile in real time. In order to monitor the processing performance, the approach should have the capability of real-time measurement. Optical coherence tomography (OCT) is an optical imaging method based on interferometer scheme.[10,11] In OCT technique, the axial resolution is inversely proportional to the bandwidth of the light source, and the lateral resolution is constrained by the optical diffraction limit. Most interest in OCT research is focused on the imaging of biomedical tissue.[12] By using the optical scanner, OCT could obtain the cross-sectional profile and the 3D structure of the tissue in real time with typical lateral and axial resolution of approximately ten microns and an imaging range of millimeters. In the same way, OCT could offer the morphological measurement in the application of manufacturing process.[13,14]

In this paper, we propose a line-field Fourier-domain interferometric method (LFI), which combines the line-field microscope with spectral interferometer, for the cross-sectional profile measurement with no scan needed. For this method, the measurement could be implemented in real-time display, and the resolution could reach $\sim 1\,\mu$m. A two-dimensional camera is used to acquire the interferogram, in which one dimension is corresponding to the microscopic imaging of the line on sample, and the other dimension is the spectrum which contains the height information of the line on sample surface. So a cross-sectional profile could be obtained just by one capture of the camera, and real-time acquisition could be easily achieved with no scan needed. The similar scheme has been introduced for the measurement of topography, and also emerged as the parallel Fourier-domain optical coherence tomography for 3D imaging of biological tissue.[15−21] However, in these prior works, both the axial and the lateral resolution were $\sim 10\,\mu$m. To increase the application potential in manufacturing process, the profile measurement should be provided in real-time display and with high resolution simultaneously. In our home-made scheme, the ultra-wide spectrum of the white light and a pair of objectives were employed to offer higher axial and lateral resolution, respectively. In spectral domain system, the height information should be reconstructed by Fourier transform algorithm from the spectrum. The use of interpolation algorithm and Fourier transform require a long time to process the large data-set, therefore the display rate is often much slower than the acquisition rate.[22−24] In this paper, graphics processing unit (GPU) has also been used to achieve the real-time reconstruction of the cross-sectional profile. As a demonstration, the cross-sectional profiles of a microfluidic chip were test.

2. Methods

2.1. *Optical scheme*

The schematic diagram of the LFI system is shown in Fig. 1. The system employs a tungsten halogen light source (Avantes, AvaLight-HAL) with an output power of 10 mW. After collimated by an achromatic lens, the light was converged in horizontal direction by a cylinder lens which was placed at its focus plane, so that a line-field illumination could be implemented on the sample. The halogen light source is difficult to focus, so a slit at focus plane of the cylindrical lens had to be used to produce more narrow line size. The light was split into the reference and sample beams by a beam splitter that is coated at the visible wavelength range, and then light was converged by a pair of $10\times/0.3$ NA objectives (Olympus, UMPLFLN10XW) to a silver coated mirror in the reference arm and the sample surface in the sample arm, respectively. The reflected light from the reference and sample beams were combined by the same beam splitter. Then the interference signal of the line pattern was projected on a grating, and finally the spectral interferogram was received by a two-dimensional camera (Silicon Imaging, SI-1300-M-CL, with 1280×1024 pixels and $5.2\,\mu$m pitch size).

J. Innov. Opt. Health Sci. 2012.05. Downloaded from www.worldscientific.com
by HUAZHONG UNIVERSITY OF SCIENCE AND TECHNOLOGY on 10/24/18. Re-use and distribution is strictly not permitted, except for Open Access articles.

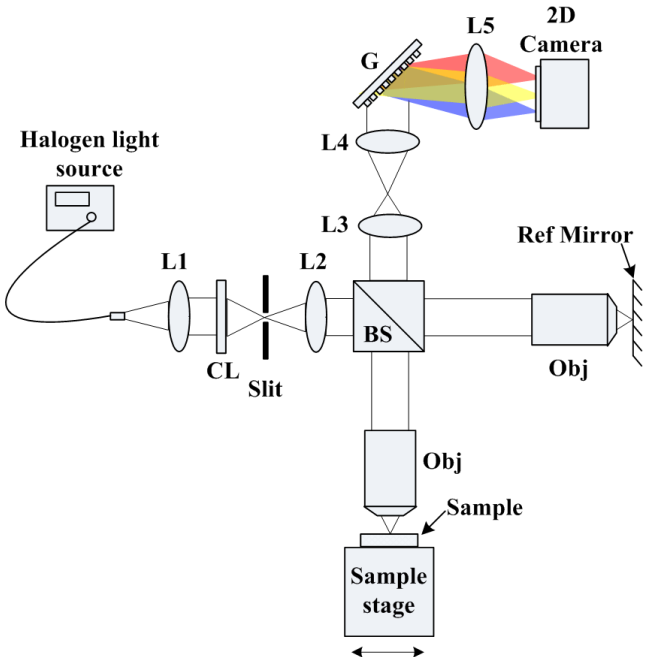

Fig. 1. The schematic diagram of the LFI system. L1: achromatic lens, $f = 50$ mm; CL: cylinder lens, $f = 200$ mm; L2−L4: achromatic lens, $f = 200$ mm; Obj: objective, 10×/0.3 NA; G: grating, 1200 l/mm; L5: achromatic lens, $f = 60$ mm.

Figure 2 shows the perspective of the optical path of the system setup. In vertical direction, the optical path was demonstrated as the line-field microscopy which is projected on the dimension of camera with 1024 pixels, and we defined the coordinate parallel to the line illumination as Y direction. In the horizontal direction, the spectrum of each point of the line illumination was split by the grating, and then projected on the dimension of camera with 1280 pixels. The height information of each point could be reconstructed by Fourier transform from the spectrum. Therefore, a B-scan was finished by one capture of the camera, and the cross-sectional profile could be reconstructed from the spectral interferogram. We define the coordinate perpendicular to the line illumination as X direction. Only one-dimensional scanning in X direction is required to achieve 3D shape measurement. In our system setup, the sample was placed on a PZT stage (Physik Instrument, P-563.3CD) for the scanning.

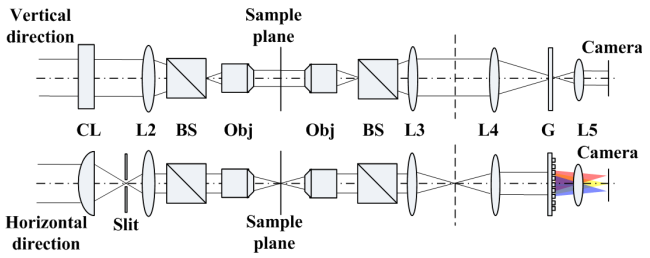

Fig. 2. Optical path of the orthogonal direction of the system setup. The abbreviation of the optical components is the same as in Fig. 1.

2.2. *Principle of height measurement*

Out of the Michelson interferometer, the interference signal I_d could be expressed as[11]:

$$I_d = 0.5(I_r + I_s) + \mathrm{Re}\{\langle E_r^*(t+\tau)E_s(t)\rangle\}. \quad (1)$$

I_r and I_s are the mean intensity from reference beam and sample beam, respectively. The second term of Eq. (1) represents the amplitude of the interference fringes which carry the information from the specimen. τ is the optical time delay between the two interference beams.

When the specimen is assumed to be an ideal mirror, the second term of Eq. (1) is:

$$\mathrm{Re}\{\langle E_r^*(t+\tau) + E_s(t)\rangle\} = |G(\tau)|\cos[\omega_0\tau + \phi(\tau)], \quad (2)$$

where ω is the frequency of the light source, $\phi(\tau)$ is the phase difference between two beams, and $G(\tau)$ is complex temporal coherence function. According to the Wiener−Khinchin theorem, $G(\tau)$ is related to the power spectrum of light source $S(\omega)$ as:

$$G(\tau) = \int_0^\infty S(\omega)\exp(-j\,\omega\tau)d\omega. \quad (3)$$

The light source in our experiment is approximately in Gaussian shape:

$$S(\omega) = \frac{4\sqrt{\ln 2\cdot\pi}}{\Delta\omega}\exp\left[-4\ln 2\left(\frac{\omega-\omega_0}{\Delta\omega}\right)^2\right]. \quad (4)$$

Therefore, the $G(\tau)$ is also in Gaussian shape:

$$G(\tau) = \exp\left[-\left(\frac{\Delta\omega\tau}{4\sqrt{\ln 2}}\right)^2\right]\exp(-j\,\omega_0\tau), \quad (5)$$

where ω_0 is center frequency of the light source, $\Delta\omega$ is full wave at half-maximum (FWHM, Full Width at Half-Maximum). So the coherence length of light source is (have been divided by 2 to take into account the double pass in the interference beam):

$$l_c = \frac{4c\ln(2)}{\Delta\omega} = \frac{2\ln 2}{\pi}\frac{\lambda_0^2}{\Delta\lambda'}, \quad (6)$$

J. Innov. Opt. Health Sci. 2012.05. Downloaded from www.worldscientific.com
by HUAZHONG UNIVERSITY OF SCIENCE AND TECHNOLOGY on 10/24/18. Re-use and distribution is strictly not permitted, except for Open Access articles.

where λ_0 is central wavelength of the light source; $\Delta\lambda'$ is the FWHM of the light source in wavelength space.

In spectral domain, the spectral information of the interference signal detected could be expressed as:

$$I(k) = I_s(k) + I_r(k) + 2\sqrt{I_s(k)I_r(k)}\mathrm{Re}\{\mu(k)e^{i[\phi_s(k)-\phi_r(k)]}\}, \quad (7)$$

where k is the wavelength number; $I_r(k)$ and $I_s(k)$ are the power spectrum of reference beam and sample beam, respectively. $\mu(k)$ is the degree of coherence (if light source is monochromatic source, $\mu(k) = 1$). $\phi_r(k)$ and $\phi_s(k)$ are spectral phase of reference beam and sample beam, respectively. The depth resolved structural data are obtained from the Fourier transform of $I(z)$ into the time domain interference pattern $I(t)$[12,25]:

$$F(z) \propto FT(I(k)). \quad (8)$$

According to the analysis above in Eq. (3), the signal fringe of $F(z)$ remains in Gaussian shape. In experiment, $I(k)$ should be a series of N discrete data. Thus, the Fourier transform could be achieved by discrete Fourier transform. The result of $F(z)$ is composed of $N/2$ discrete steps with interval size of δz (have been divided by 2 to take into account the double pass in the interference beam):

$$\delta z = \frac{\pi}{\Delta k}, \Delta k = 2\pi\frac{\Delta\lambda}{\lambda_0^2}, \quad (9)$$

where Δk is bandwidth of wavelength number; λ_0 is the detected center wavelength; and $\Delta\lambda$ is the bandwidth detected by the camera. The depth range that could be measured is (have been divided by 2 to take into account the double pass in the interference beam):

$$\Delta z = \delta z \cdot \frac{N}{2} = \frac{N}{2} \cdot \frac{\lambda_0^2}{2\Delta\lambda} = \frac{1}{4} \cdot \frac{\lambda_0^2}{\delta\lambda}, \quad (10)$$

where N is the pixel number of the camera in the dimension of spectrum collected (1280 pixels), and $\delta\lambda$ is spectral resolution of the spectrometer.

To illustrate the LFI method, a tilted slide was imaged as a sample. The interferogram acquired by the two-dimensional camera is shown in Fig. 3(a). In Fig. 3(a), the coordinate of Y is corresponding to the vertical direction of Fig. 2; the coordinate of spectrum is corresponding to the horizontal direction of Fig. 2. After Fourier transform of the interferogram at spectrum direction, the cross-sectional profile of the tilted slide was obtained, which is shown in Fig. 3(b). In our system setup,

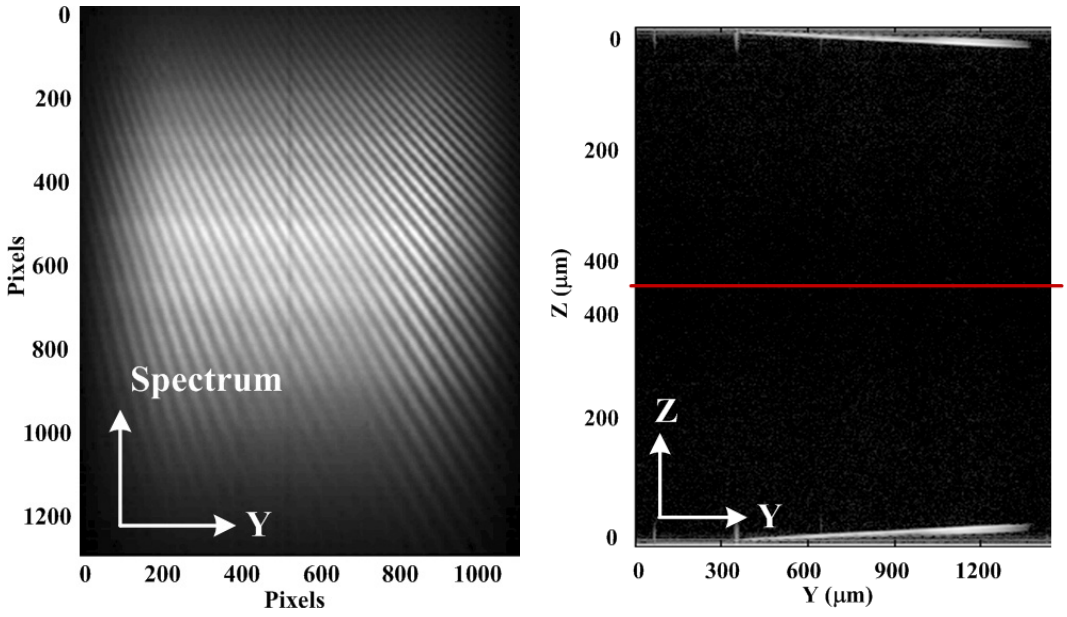

Fig. 3. The interferogram acquired by two-dimensional detector with a tilted glass as sample (a) and its reconstructed image (b). Red line is the zero-phase delay line.

J. Innov. Opt. Health Sci. 2012.05. Downloaded from www.worldscientific.com
by HUAZHONG UNIVERSITY OF SCIENCE AND TECHNOLOGY on 10/24/18. Re-use and distribution is strictly not permitted, except for Open Access articles.

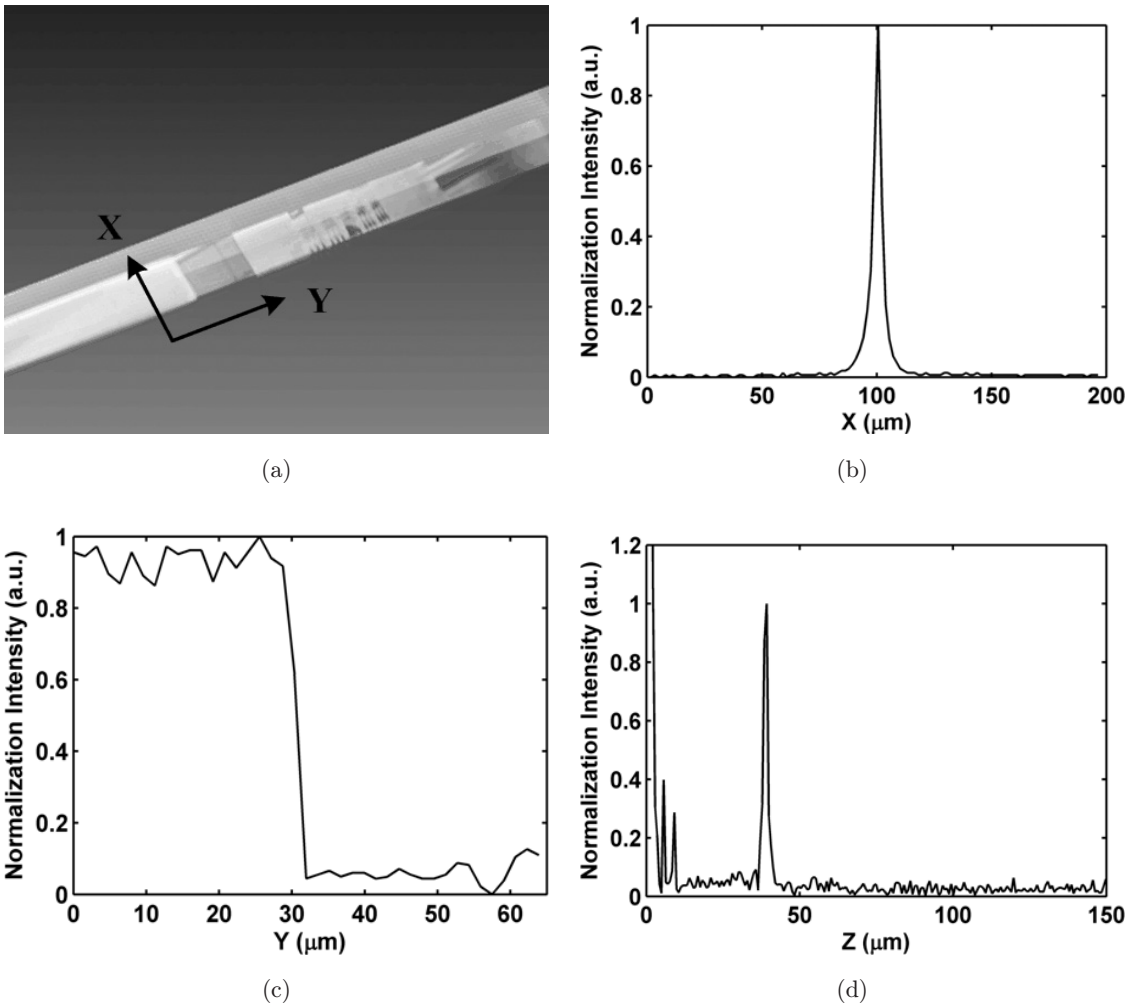

Fig. 4. (a) The 3D image of the reconstructed image of the 1951 USAF glass slide resolution target; (b) The measured lateral resolution in X direction is $\sim 8\,\mu$m; in Y direction is $\sim 3.2\,\mu$m; (c) The measured axial resolution is $\sim 1.4\,\mu$m.

the bandwidth detected is 300 nm, and then the spectral resolution is 0.234 nm, so according to Eqs. (9) and (10), the interval size δz and depth range Δz is $\sim 0.7\,\mu$m and $\sim 476\,\mu$m, respectively. The Fourier transform of a real valued function is Hermitian symmetric, so there is a mirror image on the other side of the zero-phase delay line in Fig. 3(b).[26,27] In this case, we usually take upper half space of the image.

2.3. *Data processing*

In experiment, the spectral interference signal is a series of 1280 discrete data with uneven distribution of k value. So cubic spline interpolation was used for the rescaling of the data from linear wavelength distribution to the linear k distribution. The cubic spline interpolation and Fourier transform algorithm require a long time to process the large dataset, therefore the display rate is often much slower than the acquisition rate in spectral system. In LFI system, GPU was used to achieve the real-time display of the surface profile. The program for GPU computing is programmed by compute unified device architecture (CUDA) which is highly parallelized, and GPU can reduce the time for computing with a low cost. The instruments control and the graphical user interface (GUI) were realized by LabVIEW. Through calling a dynamic link library (DLL) in the LabVIEW, the data was transferred to the GPU for processing, including cubic spline interpolation, fast Fourier transform (FFT), and image contrast stretching. The program was compiled using Microsoft Visual Studio 2008 and tested with a commercial NVIDA GeForce GTS 250 on a PC with Intel i5 760 processing core.

J. Innov. Opt. Health Sci. 2012.05. Downloaded from www.worldscientific.com
by HUAZHONG UNIVERSITY OF SCIENCE AND TECHNOLOGY on 10/24/18. Re-use and distribution is strictly not permitted, except for Open Access articles.

3. Result and Discussion

Confirmed by the experimental test on the homemade LFI system, only ∼100 ms was required for the reconstruction of a 1024 × 1280 pixels image by GPU (the original data were in Uint 16 format). The capture capability of the camera is ∼30 frame/s, with the camera exposure time of ∼2 ms, so the actual display rate of the system is 10 frames/s.

The LFI system is different with the other microscopy systems that the resolutions in X, Y, and Z directions are independent. In other words, we could control resolutions of three directions, respectively. To characterize the resolution of the LFI system, the 3D shape of a USAF 1951 resolution target was scanned with the step size of 0.5 μm and a scanning range of 100 μm in X direction. The 3D image of the result is shown in Fig. 4(a), in which the field of view (FOV) of the line illumination is ∼1.4 mm, and the elements of group 7 are imaged. The lateral resolution in X direction is originated from the size of the line illumination, which could be adjusted by the slit in experiment setup. So we measured the width of the line illumination on the sample, independently, with the slit fixed. The result is shown in Fig. 4(b), which is ∼8 μm. The resolution in Y direction is constrained by the optical diffraction limit. By measuring the edge response of the sharp line on resolution target, the lateral resolution in Y direction is provided in Fig. 4(c), which is ∼3.2 μm. The axial resolution is inversely proportional to the bandwidth of the light source. The halogen light source has a wide wavelength range from visible light to near infrared light. Due to the response of the camera, a 250 nm FWHM bandwidth centered at 650 nm was used for the LFI system; therefore, the theoretical axial resolution is ∼0.74 μm according to Eq. (6). Figure 4(b) illustrates the measured axial resolution of ∼1.4 μm.

There was only ∼12 μW illuminated on the sample, most of the light will be blocked by the slit. Furthermore, the light will be divided into 1024 parts for each point of A scan, that is ∼11.7 nW. Due to the very low power of the light source, the corresponding theoretical sensitivity is 50 dB,[12,15] and the practice sensitivity of the system is 40 dB. The sensitivity is too low for an efficient imaging of biological tissue. However, for applications in manufacturing process, such as monitoring the processing performance, and the profile measurement, this approach should have great potential.

By using the LFI system, the cross-sectional profiles of a microfluidic chip were performed in real-time without any mechanical scan. The picture of the microfluidic chip was shown in Fig. 5(a). There were two orthogonal channels on the chip, and the channels were regular rectangle engraved

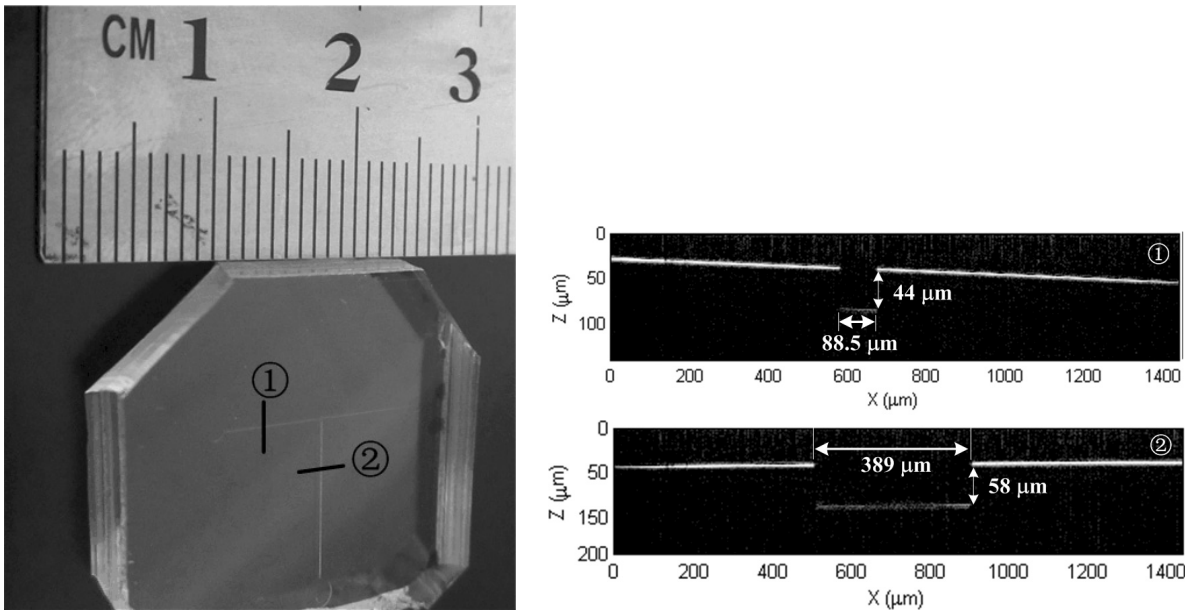

(a) (b)

Fig. 5. (a) The picture of the microfluidic chip and (b) its cross-sectional profile image.

J. Innov. Opt. Health Sci. 2012.05. Downloaded from www.worldscientific.com
by HUAZHONG UNIVERSITY OF SCIENCE AND TECHNOLOGY on 10/24/18. Re-use and distribution is strictly not permitted, except for Open Access articles.

on the transparent gel. The cross-sectional profiles of channel ① and ② were shown in Fig. 5(b) and the measured results were provided. The channel ① has a height of 44 μm, and width of 88.5 μm. The channel ② is a little bigger, that has a height of 58 μm, and width of 389 μm.

Through the experiments, the LFI system has realized the high resolution and real-time display of the cross-sectional profiles. The axial resolution is $\sim$1.4 μm, and the lateral resolution in X and Y directions could be probably enhanced by narrowing the slit and microscopy design, respectively. The FOV in X direction is decided by scanning range, and the FOV in Y direction is $\sim$1.4 mm in the experiment. However, due to the limited focus depth of the objective and the low power of light source, the actual measurement range in axial direction is $\sim$200 μm. Out of this range, the signal intensity will be too weak to recognize. To increase the imaging depth, dynamic focus technique[28] and the technique to optimize the focus condition[29] could be used in future works.

4. Conclusion

To increase the application potential in manufacturing process, such as monitoring the processing performance, the profile measurement should be provided in real-time display and with high resolution simultaneously. In this paper, we propose a LFI method for the cross-sectional profile measurement. By combining line-field microscope with spectral interferometer, a cross-sectional profile could be obtained just by one capture of the camera with no scan needed. GPU has also been used to accelerate reconstruction algorithm, and the actual displaying rate of the cross-sectional profile is 10 frames/s in experiment. The ultra-wide spectrum of the white light and a pair of objectives were used to offer high axial and lateral resolution, respectively. Through experiment test, the resolutions of the LFI system in X, Y, and Z directions are $\sim$8 μm, $\sim$3.2 μm, and $\sim$1.4 μm, respectively. As a demonstration, the cross-sectional profiles of a microfluidic chip were tested.

Acknowledgments

The work is supported by National Natural Science Foundation of China (No. 61178077) and Program for New Century Excellent Talents in University (No. NCET-08-0216).

References

1. C.-S. Lin, G.-H. Loh, S.-H. Fu, S.-W. Yang, H.-K. Chang, M.-S. Yeh, "An automatic evaluation method for the surface profile of a microlens array using an optical interferometric microscope," *Meas. Sci. Technol.* **21**, 105304 (2010).
2. S. T. Koev, R. Ghodssi, "Advanced interferometric profile measurements through refractive media," *Rev. Sci. Instrum.* **79**, 093702 (2008).
3. S. K. Debnath, M. P. Kothiyal, J. Schmit, P. Hariharan, "Spectrally resolved white-light phase-shifting interference microscopy for thickness-profile measurements of transparent thin film layers on patterned substrates," *Opt. Express* **14**, 4662 (2006).
4. Y. Kim, E. S. Choia, W. Kwak, Y. Shin, W. Jung, Y.-C. Ahn, Z. Chen, "Three-dimensional non-destructive optical evaluation of laser-processing performance using optical coherence tomography," *Opt. Laser Technol.* **40**, 625−631 (2008).
5. M. Roy, I. Cooper, P. Moore, C. J. R. Sheppard, P. Hariharan, "White-light interference microscopy: Effects of multiple reflections within a surface film," *Opt. Express* **13**, 164−170 (2005).
6. C. O'Mahony, M. Hill, M. Brunet, R. Duane, A. Mathewson, "Characterization of micromechanical structures using white-light interferometry," *Meas. Sci. Technol.* **14**, 1807−1814 (2003).
7. J. Schmit, A. Olszak, "High-precision shape measurement by white-light interferometry with real-time scanner error correction," *Appl. Opt.* **41**, 5943−5950 (2002).
8. K. G. Larkin, "Efficient nonlinear algorithm for envelope detection in white light interferometry," *J. Opt. Soc. Am. A* **13**, 832−843 (1996).
9. P. D. Groot, L. Deck, "Surface profiling by analysis of white-light interferograms in the spatial frequency domain," *J. Mod. Opt.* **42**, 389−401 (1995).
10. D. Huang, E. A. Swanson, C. P. Lin, J. S. Schuman, W. G. Stinson, W. Chang, M. R. Hee, T. Flotte, K. Gregory, C. A. Puliafito *et al.*, "Optical coherence tomography," *Science* **254**, 1178−1181 (1991).
11. J. M. Schmitt, "Optical coherence tomography (OCT): A review," *IEEE J. Sel. Top. Quant.* **5**, 1205−1215 (1999).
12. A. F. Fercher, W. Drexler, C. K. Hitzenberger, T. Lasser. "Optical coherence tomography-principles and applications," *Rep. Prog. Phys.* **66**, 239−303 (2003).
13. D. Stifter, "Beyond biomedicine: A review of alternative applications and developments for

J. Innov. Opt. Health Sci. 2012.05. Downloaded from www.worldscientific.com
by HUAZHONG UNIVERSITY OF SCIENCE AND TECHNOLOGY on 10/24/18. Re-use and distribution is strictly not permitted, except for Open Access articles.

optical coherence tomography," *Appl. Phys. B* **88**, 337−357 (2007).
14. X. Li, G. Shi, L. Wei, Z. Ding, Y. Zhang, "High-speed spectral domain optical coherence tomography signal processing with time-domain interpolation using graphics processing unit," *J. Innov. Opt. Health Sci.* **3**, 325−335 (2011).
15. B. Grajciar, M. Pircher, A. F. Fercher, R. A. Leitgeb, "Parallel Fourier domain optical coherence tomography for *in vivo* measurement of the human eye," *Opt. Express* **13**, 1131−1137 (2005).
16. T. Endo, Y. Yasuno, S. Makita, M. Itoh, T. Yatagai, "Profilometry with line-field Fourier-domain interferometry," *Opt. Express* **13**, 695−701 (2005).
17. M. Bhattacharjee, P. C. Ashok, K. Divakar Rao, S. K. Majumder, Y. Verma, P. K. Gupta, "Binary tissue classification studies on resected human breast tissues using optical coherence tomography images," *J. Innov. Opt. Health Sci.* **1**, 59−66 (2011).
18. S.-W. Lee, B.-M. Kim. "Line-field optical coherence tomography using frequency-sweeping source," *IEEE J. Quant. Elect.* **14**, 50−55 (2008).
19. Y. Nakamura, S. Makita, M. Yamanari, M. Itoh, T. Yatagai, Y. Yasuno, "High-speed three-dimensional human retinal imaging by line-field spectral domain optical coherence tomography," *Opt. Express* **15**, 7103−7116 (2007).
20. Y. Yasuno, T. Endo, S. Makita, G. Aoki, M. Itoh, T. Yatagai, "Three-dimensional line-field Fourier domain optical coherence tomography for in vivo dermatological investigation," *J. Biomed. Opt.* **11**, 014014 (2006).
21. R. N. Graf, W. J. Brown, A. Wax, "Parallel frequency-domain optical coherence tomography scatter-mode imaging of the hamster cheek pouch using a thermal light source," *Opt. Lett.* **33**, 1285−1287 (2008).
22. K. Zhang, J. U. Kang, "Real-time 4D signal processing and visualization using graphics processing unit on a regular nonlinear-k Fourier-domain OCT system," *Opt. Express* **18**, 11,772−11,784 (2010).
23. Y. Watanabe, T. Itagaki, "Real-time display on Fourier domain optical coherence tomography system using a graphics processing unit," *J. Biomed Opt.* **14**, 060506 (2009).
24. S. Ver Jeught, A. Bradu, A. Gh. Podoleanu, "Real-time resampling in Fourier domain optical coherence tomography using a graphics processing unit," *J. Biomed. Opt.* **15**, 030511 (2010).
25. A. F. Fercher, C. K. Hitzenberger, G. Kamp, S. Y. El-Zaiat, "Measurement of intraocular distances by backscattering spectral interferometry," *Opt. Commun.* **117**, 43−48 (1995).
26. R. K. Wang, "*In vivo* full range complex Fourier domain optical coherence tomography," *Appl. Phys. Lett.* **90**, 05413 (2007).
27. R. K. Wang, "Fourier domain optical coherence tomography achieves full range complex imaging *in vivo* by introducing a carrier frequency during scanning," *Phys. Med. Biol.* **52**, 5897−5907 (2007).
28. S. Murali, K. S. Lee, J. P. Rolland, "Invariant resolution dynamic focus OCM based on liquid crystal lens," *Opt. Express* **15**, 15854−15862 (2007).
29. L. Liu, C. Liu, W. C. Howe, C. J. R. Sheppard, N. Chen, "Binary-phase spatial filter for real-time swept-source optical coherence microscopy," *Opt. Lett.* **32**, 2375−2377 (2007).